Equivalent Circuit Model for a THz Detector Based on the Double-Electron Layer Tunneling Transistor (DELTT)

Majid M. Khodier, *Member, IEEE*, Christos G. Christodoulou, *Fellow, IEEE*, and Jerry A. Simmons

***Abstract*—An equivalent circuit model for the double-electron layer tunneling transistor (DELTT) integrated with an antenna is presented in this paper. This device is used basically for THz detection, and the antenna is used to efficiently couple THz radiation into the device for processing. Developing an equivalent circuit model is extremely helpful in matching the antenna to the device.**

***Index Terms*—Circuit model, double-electron layer tunneling transistor (DELTT), THz detector.**

I. Introduction

SINCE the first theoretical work on GaAs–AlGaAs superlattices and experimental work on resonant tunneling (RT) double-barrier, and later triple-barrier heterostructures, there has been much interest in these devices for high frequency applications in oscillators, detectors, switches, etc. Attracted by the high-frequency detection and room-temperature operation of the RT device, theoretical investigation as well experimental work have been performed to study the device [1].

In the last decade, there has been much interest in realizing THz detectors based on the idea of photon-assisted tunneling (PAT) between confined states inside double-quantum well (DQW) device, and considerable work has been done in this direction [2]–[5]. A proposed THz detector, utilizing two-dimensional–two-dimensional (2-D–2-D) PAT in double quantum wells, has the structure depicted in Fig. 1. The core of the detector is a double-electron layer tunneling transistor (DELTT), the first quantum tunneling transistor whose behavior is not sensitive to lateral dimensions of the device, and the only critical dimension is the vertical growth direction. The DELTT is typically fabricated from a modulation-doped DQW heterostructure, made from $Al_{0.3}Ga_{0.7}As/GaAs$ material system. A complete review of the principle of operation of the device can be found in [4]. Since the active area of the DELTT structure is very small, alone it is not efficient in collecting THz radiation, and an antenna is needed to increase the coupling efficiency. The bowtie antenna structure is chosen to be integrated with the device because of its broadband characteristic, easy design, and compatibility with the detector fabrication process. The resultant structure of the THz detector is shown in Fig. 1.

Manuscript received December 19, 2001; revised June 19, 2002. The review of this paper was arranged by Editor S. Datta

M. M. Khodier and C. G. Christodoulou are with the Department of Electrical and Computer Engineering, University of New Mexico, Albuquerque, NM 87131 USA (e-mail: mkhod@eece.unm.edu).

J. A. Simmons is with Sandia National Laboratories, Albuquerque, NM 87185-1415 USA.

Publisher Item Identifier 10.1109/TED.2002.803641.

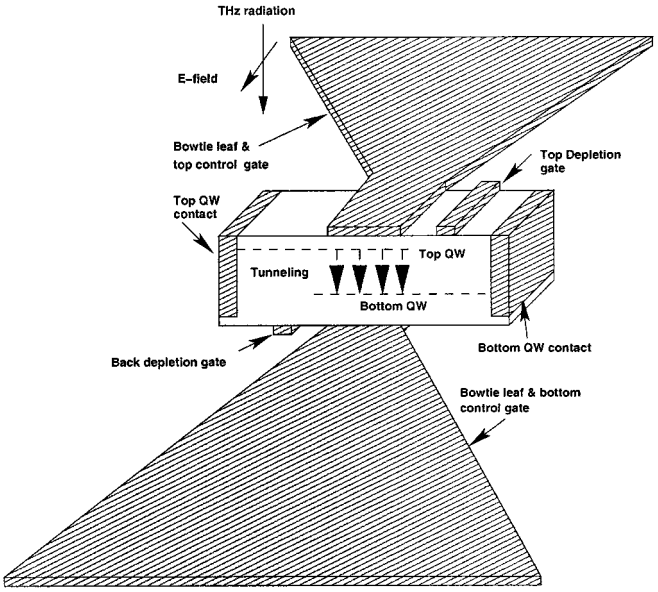

Fig. 1. Overview of the DQW THz detector integrated with a bowtie antenna. The top and bottom bows are connected to the top and bottom control gates, respectively. The control gates are used to change the density of electrons in each QW, and therefore provide the electrical tunable characteristic through a dc bias. The depletion gates are used to deplete the QW the one does not wish to contact. The top QW contact is called the source, and the bottom QW contact is called the drain. The structure without the bowtie antenna is called DELTT.

In order to achieve maximum coupling between the device and the incoming beam, the device impedance should be equal to the complex conjugate of the antenna impedance. For this purpose, a method to estimate the frequency dependent impedance of the DQW well device is required. This can be achieved by developing an equivalent circuit model of the device which incorporates all the important physical processes and geometrical dimensions that affect the device operation.

A lumped circuit model for the DELTT, valid at dc, is presented in [6]. Another equivalent circuit model for a single 2-D electron gas (2-DEG), which is capacitively contacted to metallic gates was presented in [7], based on the concept of kinetic inductance. The circuit model consists of either lumped elements or distributed elements (i.e., transmission line), depending on the structure dimensions. The validity of the model at microwave frequencies was also experimentally verified in [7]. In [8], an equivalent model for a DQW was developed using transmission line theory. However, the model did not take into consideration the presence of a gate on top or below (or both) of the DQW structure. The subject of this paper is to develop a general equivalent circuit model for the

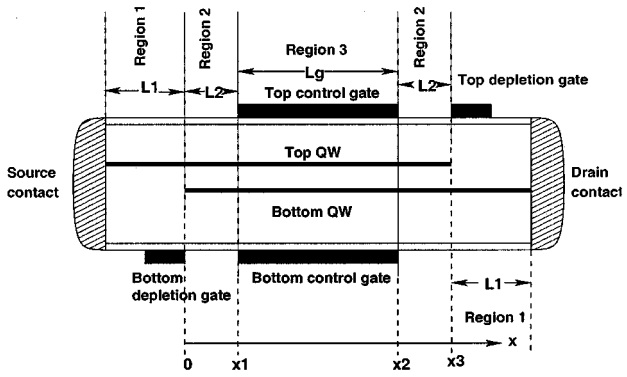

Fig. 2. Cross section of the DELTT showing the three regions used in the calculation of the equivalent circuit.

DELTT structure, which has both top and bottom gates. This work represents an extension to the work found in [7] and [8] to include the effect of the top and bottom gates.

Using the equivalent circuit models in [6]–[8], and the one developed in this paper, circuit models for more complex geometries can be easily built by connecting these simple circuit models in series or parallel.

II. Kinetic Inductance of Electrons Inside a 2-DEG

The Drude model for the frequency dependent resistivity of a single 2-DEG layer is [7]

$$\rho(\omega) = \frac{m^*}{ne^2\tau_{\rm mom}}\left(1 + j\omega\tau_{\rm mom}\right) \tag{1}$$

where n is the electron density, e the electron charge, m^* the effective mass, and $\tau_{\rm mom}$ the momentum scattering time. Equation (1) is the sum of a real part, which is the resistance, and a positive, frequency-dependent, imaginary part, which can be considered as an inductive reactance. This inductance is known as the kinetic inductance, because the inductive energy is stored in the kinetic energy of the electrons. At low frequencies, the imaginary part of ρ is very small and usually neglected when developing circuit models for the 2-DEG. At THz frequencies, however, the imaginary part becomes dominant, and it is necessary to include in any circuit model. It should be mentioned that the momentum scattering time $\tau_{\rm mom}$ in modulation doped MBE-grown, high-mobility GaAs/AlGaAs structures at low temperatures (<4 K) is 3–4 orders of magnitude larger than in conventional, bulk doped semiconductors at room temperature.

To ease the calculation of the equivalent circuit model for the DELTT, its cross section is divided into three different regions, as shown in Fig. 2. These regions are as follows.

- Region 1: This region consists of a section of either the top or the bottom QW, and extends from the source (or drain) contact to the end of the bottom (or top) depletion gate. In this region, there is no tunneling. The equivalent circuit for this region is composed basically of a resistance in series with inductance. The length of this regions is L_1.
- Region 2: This region consists of the section of the DELTT between the control gates and the depletions gates where there is overlap between the top and the bottom QWs, and in this region tunneling can occur. The equivalent circuit for this region is a transmission line of length L_2. An incremental length of this region consists of a resistance R in series with an inductance L, to model each QW, and a shunt capacitance C and conductance G to model the capacitance and the tunneling conductance between the top and bottom QWs. The values of the elements in this region are per unit length.
- Region 3: This region consists of the section of the DELTT where there is overlap between the top and bottom QWs, and covered by the top and bottom control gates, and in this region tunneling can occur. The equivalent circuit for this region is also a transmission line of length L_g. An incremental length of this region has a similar circuit as that of region 2, but with an extra top and bottom capacitors, C_t and C_b, to model the contact capacitances between the top control gate and top QW, and between the bottom control gate and bottom QW, respectively. The values of the elements in this region are per unit length.

It should be mentioned that the DELTT structure studied here is symmetrical, i.e., electron densities in both QWs are the same. The overall equivalent circuit model for the DELTT transistor, with an antenna connected between the top and bottom control gates, is shown in Fig. 3. In terms of mobility μ, areal density n, the width w, dielectric permittivity ϵ of the material between the QWs, and distance between the two QWs d_{qw}, R, L, and C in Fig. 3 are given by

$$R = \frac{1}{en\mu w} \tag{2}$$

$$L = \frac{m^*}{e^2 n w} \tag{3}$$

$$C = \epsilon \times \frac{d_{qw}}{w}. \tag{4}$$

The small signal tunneling conductance G can be obtained from the I–V curve of the DELTT by taking the derivative of the current with respect to the applied bias. The element values R_s, L_s, R_d, and L_d shown in Fig. 3 can be calculated from (2) and (3) by multiplying the result from each equation by the length L_1. The remaining elements, C_t and C_b, represent the geometrical capacitance between the top gate and the top QW and that between the bottom gate and bottom QW, respectively, and can be calculated as follows:

$$C_t = \epsilon \times \frac{d_t}{w} \tag{5}$$

$$C_b = \epsilon \times \frac{d_b}{w} \tag{6}$$

where d_t and d_b are the distances between the top gate and the top QW, and the bottom gate and bottom QW, respectively, and ϵ is the dielectric permittivity of the material between each gate and the corresponding QW. The antenna is modeled as a current source $I_{\rm ant}$ in parallel with the antenna impedance $Z_{\rm ant}$ as shown in Fig. 3. The current source $I_{\rm ant}$ is related to the antenna directivity, radiation resistance, and the incident power through the following relation [9]:

$$I_{\rm ant} = \sqrt{\frac{2DP_{\rm in}}{\pi R_r}} \tag{7}$$

where D is the antenna directivity, R_r is the radiation resistance, and $P_{\rm in}$ is the incident power. We should mention that before the equivalent circuit model of the device was developed, an extensive static analysis (based on the numerical solution of Poisson's

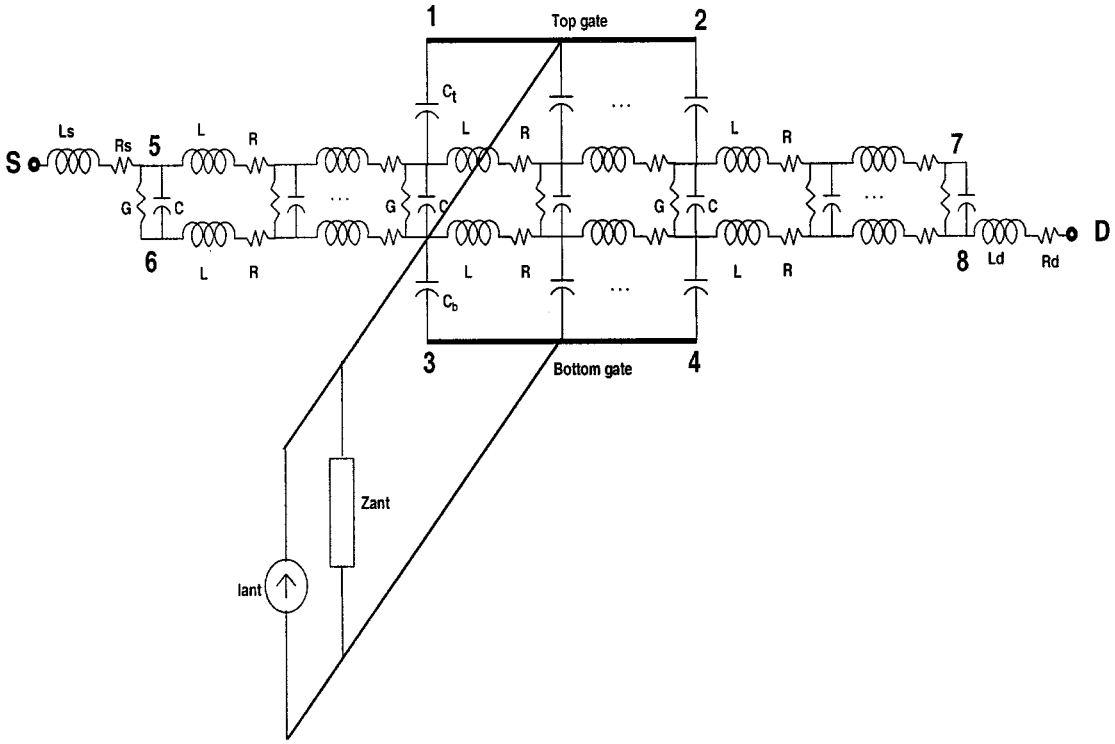

Fig. 3. Equivalent circuit model of the DELTT with an antenna connected between the top and bottom control gates.

equation) and full-wave electromagnetic simulations using the finite difference time domain (FDTD) method, were performed on the device structure. The purpose of these simulations was to investigate the electric field distributions inside the device both as a function of frequency and the dc voltage applied to the gates or the source and drain. Based on these simulations and other published work, we decided that the simplest, and yet accurate, equivalent circuit model for our device is the one shown in Fig. 3.

III. Analysis of the Equivalent Circuit

It is clear that the circuit model as depicted in Fig. 3 is very complex and difficult to analyze. The analysis can even be more complicated if the condition of symmetrical QWs is relaxed, and the effect of the control gates voltages on the electron density in each QW is taken into consideration. It should be mentioned here that we attempt to develop a first-order circuit model for the DELTT that incorporates the most important parameters of the device (gate width, electron density, separation between the gates and the QWs, and the separation between the QWs themselves, etc.) We also tried to make the circuit model semi-analytical as much as possible. Measurements on a single QW with a top gate in the frequency range 1–10 GHz [7] showed a good agreement with a circuit model similar to ours, without including the discontinuity effects. Moreover, since in our device the separation between the gates and the QWs is very small ($\sim$1 μm), the electric field is almost entirely distributed beneath the gate region, and the fringing field at the edges is very small (this was also verified by our full-wave simulations and static analysis). Due to these reasons, we decided that the discontinuity effects are not important in our model. Certainly, more complete and accurate models would take a serious look at these effects, especially if variations of our device are considered. The circuit model can also be improved by performing some measurements at relatively high frequencies ($\sim$50 GHz).

We can analyze the structure shown in Fig. 3 by assigning position dependent voltage and current for each transmission line, and then solve the resulting coupled differential equations. The input impedance between any two points in Fig. 3 can be found by applying the appropriate boundary conditions and solving for the unknown coefficients, and then divide the appropriate voltage and current. Before starting the analysis, the following variables are defined. For $0 \leq x \leq x_1$, we have $V_{t,l}(x)$: voltage on the top QW, $V_{b,l}(x)$: voltage on the bottom QW, $I_{t,l}(x)$: current on the top QW, $I_{b,l}(x)$: current on the bottom QW. For $x_1 \leq x \leq x_2$, we have $V_{tg}(x)$: voltage on the top control gate, $V_{bg}(x)$: voltage on the bottom control gate, $I_{tg}(x)$: current on the top control gate, $I_{bg}(x)$: current on the bottom control gate, $V_t(x)$: voltage on the top QW, $V_b(x)$: voltage on the bottom QW, $I_t(x)$: current on the top QW, $I_b(x)$: current on the bottom QW. For $x_2 \leq x \leq x_3$, we have $V_{t,r}(x)$: voltage on the top QW, $V_{b,r}(x)$: voltage on the bottom QW, $I_{t,r}(x)$: current on the top QW, and $I_{b,r}(x)$: current on the bottom QW, where $x_1 = L_2$, $x_2 = L_2 + L_g$, and $x_3 = 2L_2 + L_g$. It is also useful to define the following parameters in terms of the circuit elements shown in Fig. 3. This is useful because it reduces the notation of the resulting solution. We define: $Z = R + j\omega L$, $Y = G + j\omega C$, $\gamma = \sqrt{2(R + j\omega L)(G + j\omega C)}$ $Z_c = (1/\sqrt{2})\sqrt{(R + j\omega L)/(G + j\omega C)}$, $Y_t = j\omega C_t$, $Y_b = j\omega C_b$, $Y_1 = \sqrt{4Y^2 + Y_t^2 + Y_b^2 - 2Y_tY_b}$, $Y_2 = 2Y + Y_t + Y_b$, $\gamma_1 = (\sqrt{2}/2)[Z(Y_1 + Y_2)]^{1/2}$, and $\gamma_2 = (\sqrt{2}/2)[Z(-Y_1 + Y_2)]^{1/2}$.

It is relatively easy to formulate the transmission line equations for each region [10]–[12], and solve the resulting system of

differential equations, although the solution involves a considerable amount of mathematical manipulations. A mathematical software like Matlab or Mathematica can be used to solve the resulting differential equations for each region. The details are skipped here, and we quote only the final results.

For $0 \le x \le x_1$, we have

$$V_{t,l} = \tfrac{1}{2}\left(A_1 x + B_1 + C_1 e^{-\gamma x} + D_1 e^{\gamma x}\right) \tag{8}$$

$$I_{t,l} = \frac{1}{2Z}\left(-A_1 + \gamma C_1 e^{-\gamma x} - \gamma D_1 e^{\gamma x}\right) \tag{9}$$

$$V_{b,l} = \tfrac{1}{2}\left(A_1 x + B_1 - C_1 e^{-\gamma x} - D_1 e^{\gamma x}\right) \tag{10}$$

$$I_{b,l} = \frac{1}{2Z}\left(-A_1 - \gamma C_1 e^{-\gamma x} + \gamma D_1 e^{\gamma x}\right). \tag{11}$$

For $x_1 \le x \le x_2$, we have

$$\begin{aligned} V_t(x) = {} & \frac{1}{Y_t}\left[E_2 + Y_t E_7 + \gamma_1\left(E_3 e^{\gamma_1 x} - E_4 e^{-\gamma_1 x}\right)\right. \\ & \left. + \gamma_2\left(E_5 e^{\gamma_2 x} - E_6 e^{-\gamma_2 x}\right)\right] \end{aligned} \tag{12}$$

$$\begin{aligned} V_b(x) = {} & \frac{1}{2YY_t}\left[2(Y + Y_t)E_2 + 2YY_t E_7\right. \\ & + \gamma_1(Y_t - Y_b - Y_1)\left(E_3 e^{\gamma_1 x} - E_4 e^{-\gamma_1 x}\right) \\ & \left. + \gamma_2(Y_t - Y_b + Y_1)\left(E_5 e^{\gamma_2 x} - E_6 e^{-\gamma_2 x}\right)\right] \end{aligned} \tag{13}$$

$$V_{tg}(x) = E_7 \tag{14}$$

$$V_{bg}(x) = \left(\frac{1}{Y_t} + \frac{1}{Y_b} + \frac{1}{Y}\right)E_2 + E_7 \tag{15}$$

$$\begin{aligned} I_t(x) = {} & -\frac{1}{ZY_t}\left[\gamma_1^2\left(E_3 e^{\gamma_1 x} + E_4 e^{-\gamma_1 x}\right)\right. \\ & \left. + \gamma_2^2\left(E_5 e^{\gamma_2 x} + E_6 e^{-\gamma_2 x}\right)\right] \end{aligned} \tag{16}$$

$$\begin{aligned} I_b(x) = {} & -\frac{1}{2ZYY_t}\left[\gamma_1^2(Y_t - Y_b - Y_1)\left(E_3 e^{\gamma_1 x} + E_4 e^{-\gamma_1 x}\right)\right. \\ & \left. + \gamma_2^2(Y_t - Y_b + Y_1)\left(E_5 e^{\gamma_2 x} + E_6 e^{-\gamma_2 x}\right)\right] \end{aligned} \tag{17}$$

$$\begin{aligned} I_{tg}(x) = {} & E_1 + E_2 x + E_3 e^{\gamma_1 x} + E_4 e^{-\gamma_1 x} \\ & + E_5 e^{\gamma_2 x} + E_6 e^{-\gamma_2 x} \end{aligned} \tag{18}$$

$$\begin{aligned} I_{bg}(x) = {} & -\frac{1}{2YY_t}\left[2YY_t(E_1 - E_8) + 2YY_t E_2 x\right. \\ & + \left(Y_b^2 + Y_b Y_1 - Y_b Y_t\right)\left(E_3 e^{\gamma_1 x} + E_4 e^{-\gamma_1 x}\right) \\ & \left. - \left(Y_b^2 + Y_b Y_1 + Y_b Y_t\right)\left(E_5 e^{\gamma_2 x} + E_6 e^{-\gamma_2 x}\right)\right]. \end{aligned} \tag{19}$$

Finally, for $x_2 \le x \le x_3$, we have

$$V_{t,r} = \tfrac{1}{2}\left(A_2 x + B_2 + C_2 e^{-\gamma x} + D_2 e^{\gamma x}\right) \tag{20}$$

$$I_{t,r} = \frac{1}{2Z}\left(-A_2 + \gamma C_2 e^{-\gamma x} - \gamma D_2 e^{\gamma x}\right) \tag{21}$$

$$V_{b,r} = \tfrac{1}{2}\left(A_2 x + B_2 - C_2 e^{-\gamma x} - D_2 e^{\gamma x}\right) \tag{22}$$

$$I_{b,r} = \frac{1}{2Z}\left(-A_2 - \gamma C_2 e^{-\gamma x} + \gamma D_2 e^{\gamma x}\right). \tag{23}$$

Equations (8)–(23) contain 16 unknown coefficients, $A_{1,2}, \ldots D_{1,2}, E_1, \ldots E_8$, and we need 16 independent boundary conditions to find these coefficients. The unknown coefficients can be found by imposing the appropriate boundary conditions at $x = 0$, x_1, x_2, and x_3. For example, at $x = x_1$, the boundary conditions are: $V_{t,l} = V_t$, $I_{t,l} = I_t$, $V_{b,l} = V_b$, and $I_{b,l} = I_b$. We have similar boundary conditions at $x = x_2$.

TABLE I
SAMPLE PARAMETERS FOR DELTT DEVICES G1717 AND EA255. THE LISTED PARAMETERS ARE QW WIDTHS (w_{qw}), TUNNEL BARRIER THICKNESS (d_{qw}), ELECTRON DENSITIES FOR THE TOP AND BOTTOM QWS (n_t AND n_b), DISTANCE FROM TOP CONTROL GATE TO TOP QW (d_t) AND DISTANCE FROM BOTTOM CONTROL GATE TO BOTTOM QW (d_b), DEVICE CHANNEL WIDTH ($w_{\rm chan}$), LENGTH OF THE CONTROL GATES ($L_{\rm cg}$), LENGTH OF THE DEPLETION GATES (L_{dg}), AND THE SEPARATION BETWEEN THE CONTROL GATES AND DEPLETION GATES (L_{cg-dg})

Sample	w_{qw} (Å)	d_{qw} (Å)	n_t ($10^{11}cm^{-2}$)	n_b ($10^{11}cm^{-2}$)	d_t (μm)	d_b (μm)	w_{chan} (μm)	L_{cg} (μm)	L_{dg} (μm)	L_{cg-dg} (μm)
G1717	150	125	2.0	1.4	0.13	2.2	500	40	10	5
EA255	120	100	5.6	6.6	0.09	0.12	10	1.0	0.5	0.5

IV. NUMERICAL RESULTS AND DISCUSSION

In this section, we present numerical results for the input impedance of the DELTT between different points. Mainly, we will be concerned with impedance calculation between the source and the drain, and between the top and bottom control gates. These are the two possible locations were an antenna can be connected to the DELTT device. Sample parameters values for two DELTT devices (G1717 and EA255) will be used in the calculations, and these parameters are shown Table I. The DELTT devices used here are the same devices used in [3], and are chosen because the electron densities in the QWs are close from each other, so that a symmetrical device is assumed for impedance calculations. In all of the following results, the tunneling conductance is assumed to be zero; $G = 0$, unless mentioned otherwise. Even if the tunneling conductance is not zero, the reactance of the capacitor C will short out G at high frequencies of our interest, and the same simulation results will be obtained.

A. Calculating Z_{sd}

To calculate the input impedance between the source and the drain Z_{SD}, (8)–(23) are solved for the unknown coefficients using the boundary conditions of a voltage source at point S, and a ground at the drain, D. After finding the unknown coefficients, the input current at the source is found from (9), and then the voltage is divided by the current at the source to obtain Z_{SD}. Element values like R, L, C, C_t, C_b, R_s, R_d, L_s, and L_d are calculated from the parameters in Table I using (2)–(6). The tunneling conductance is calculated from the I–V curve of the DELTT device by evaluating the slope of the current–voltage (I–V) curve at a certain bias point.

Applying the previous procedure, we calculated Z_{SD} as a function of frequency and the result is shown in Fig. 4 for the G1717 sample. The imaginary part of Z_{SD} increases slowly with frequency because of the source and drain conductances (L_s and L_d). The results show that the high frequency limit is basically that of an inductor. Each extra peak with increasing frequency corresponds to fitting one more wavelength into the combined length of regions 2 and 3.

At this point, we want to verify the accuracy of the simulation results of the input impedance based on the implementation of (8)–(23). This is done by calculating Z_{SD} for the DELTT device but without control gates. The DELTT equivalent circuit without the top and bottom control gates is similar to that shown in Fig. 3

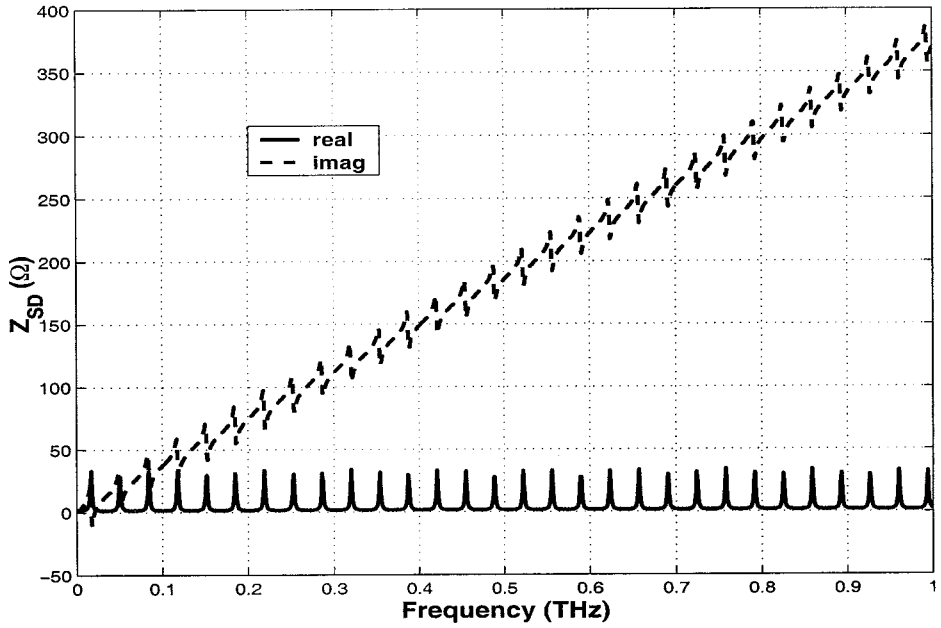

Fig. 4. Simulation results of Z_{SD} for the G1717 sample.

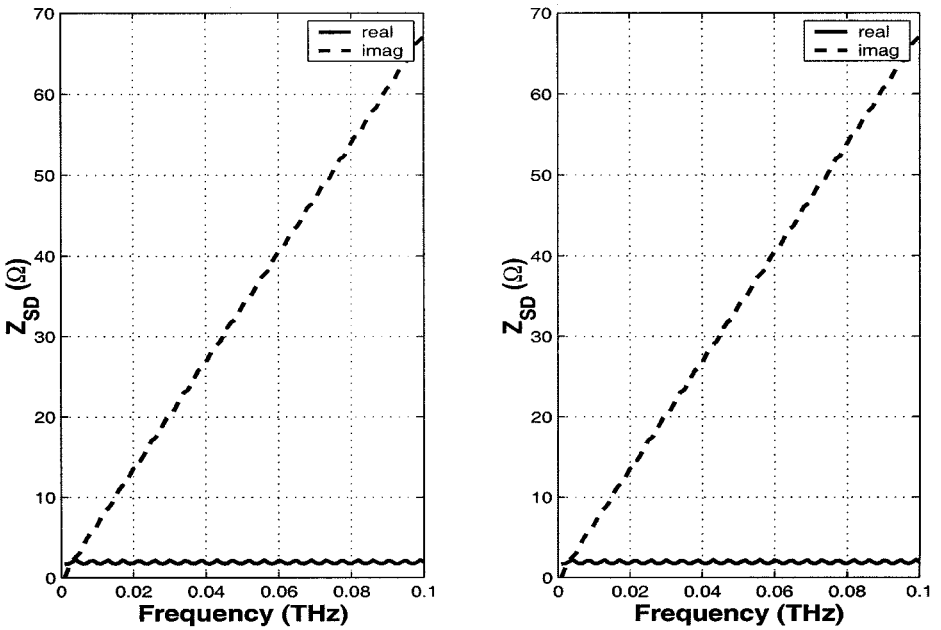

Fig. 5. Simulation results (left plot) and theoretical results (right plot) of Z_{SD} for the G1717 sample. The simulation results are obtained using d_t and $d_b = 1.0$ m.

but now C_t and C_b are zero. Therefore, the equivalent circuit of the DELTT reduces to that of a DQW (similar to the one in region 2) but now it extends from $x = 0$ to $x = x_3$. The voltages and currents that exist in the DQW structure are given by equations similar to those in (8)–(11). For this case, a closed-form solution for Z_{sd} can be obtained and it is given by [8]

$$Z_{sd} = Z_s + Z_d + \frac{x_3}{2} Z + Z_c \coth\left(\frac{\gamma x_3}{2}\right) \tag{24}$$

where $Z_s = R_s + j\omega L_s$ and $Z_d = R_d + j\omega L_d$. The DELTT structure without top and bottom control gates can be simulated by using large values of d_t and d_b so that C_t and C_b are very small as if they do not exist in the circuit model of the DELTT. The simulation results and predicted results based on (24) for this case are shown in Fig. 5. These results are virtually indistinguishable, which verifies the validity and generality of our circuit model for the DELTT structure.

The above calculations are repeated for the EA255 sample and the results are shown in Figs. 6 and 7. The dimensions of this device are much smaller than the dimensions of the G1717 device, and therefore the resonances are more separated and shifted to higher frequencies. We also note that Z_{SD} exhibits large, sharp resonance peaks (around 0.75 and 2.25 THz), surrounded by many smaller resonances. These resonances, large and small, are observed both in the real and imaginary parts of Z_{SD}, as can be seen from Fig. 6.

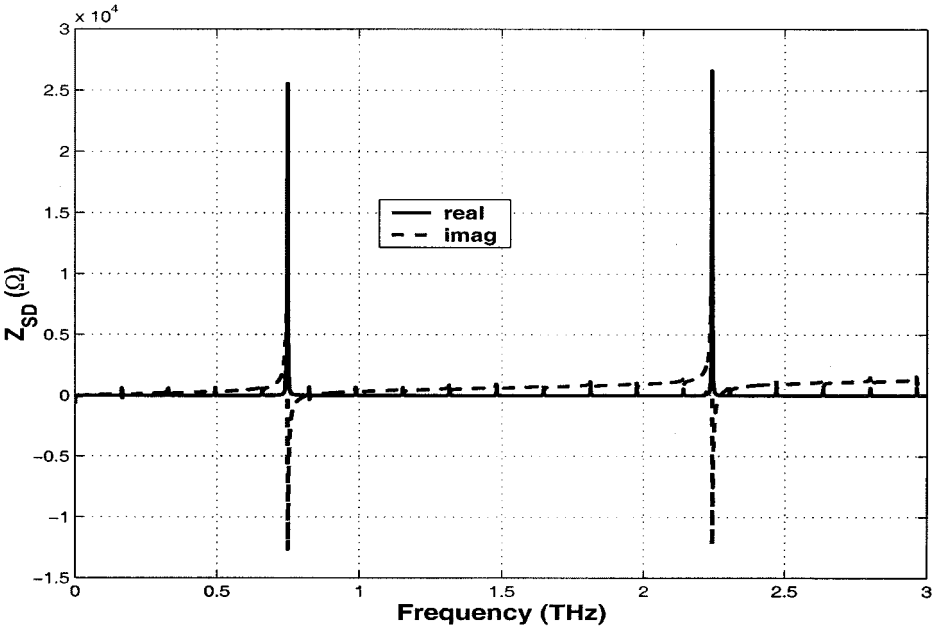

Fig. 6. Simulation results of Z_{SD} for the EA255 sample.

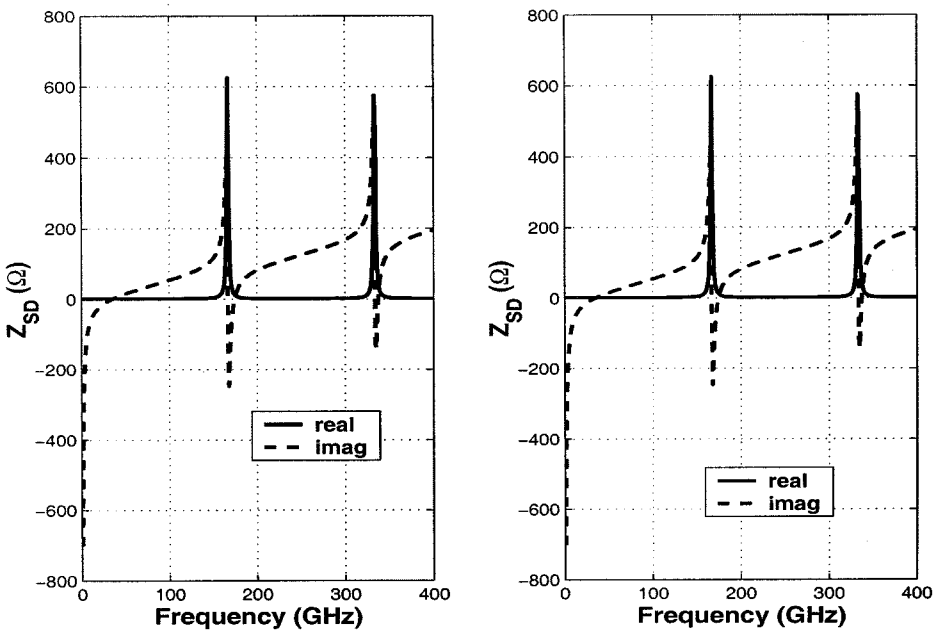

Fig. 7. Simulation results (left plot) and theoretical results (right plot) of Z_{SD} for the EA255 sample. The simulation results are obtained using d_t and $d_b = 1.0$ m.

B. Calculating Z_{13}

The impedance Z_{13} represents the impedance of the DELTT between the top and the bottom control gates where an antenna can be connected. This impedance can be calculated by applying a voltage source at point 1, grounding points 3, S, and D in Fig. 3, solving (8)–(23) for the unknown coefficients, and then dividing the voltage by the current at point 1. Simulation results for the G1717 sample are shown in Fig. 8 for different values of d_b. The input impedance Z_{13} has a very small real part (negligible and not shown in the figure), and a negative imaginary part that resembles the reactance of a capacitor. We propose that Z_{13} is simply the reactance of the series combination of the capacitors C_t, C, and C_b, and therefore Z_{13} is given by

$$Z_{13} = \frac{1}{L_{\rm cg}} \left(\frac{1}{Y} + \frac{1}{Y_t} + \frac{1}{Y_b} \right) \tag{25}$$

where $L_{\rm cg}$ is the length of the control gate(s). The calculated values of Z_{13} using (25) are also shown in Fig. 8 for different values of d_b. The simulation results and the theoretical results agree very well, which suggests that (25) is accurate enough to predict Z_{13} of the DELTT structure. Simulations and calculations are repeated for the EA255 sample, and the results are shown in Fig. 9.

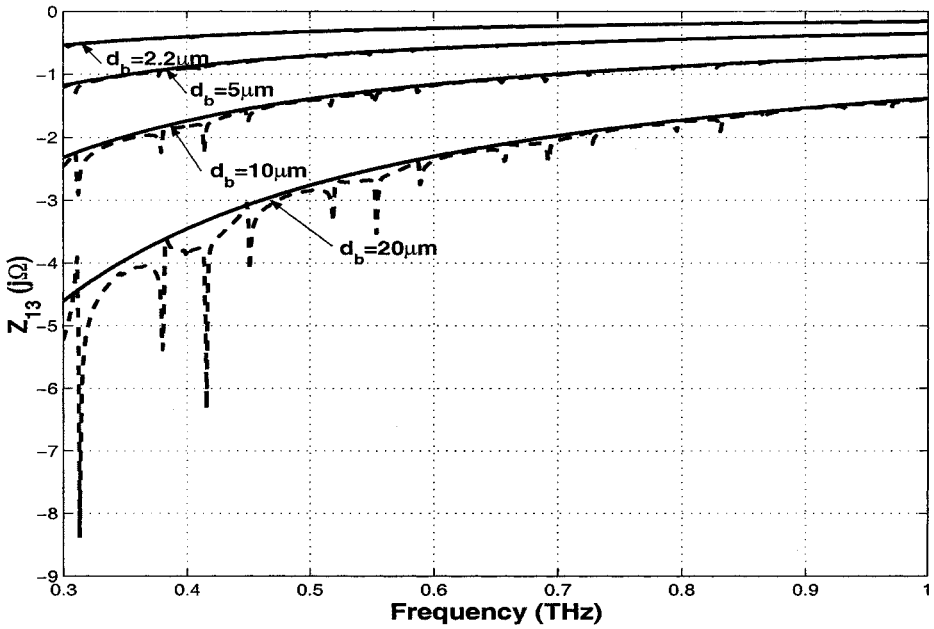

Fig. 8. Simulation (dashed line) and predicted (solid line) results of Z_{13} for the G1717 sample at different values of d_b.

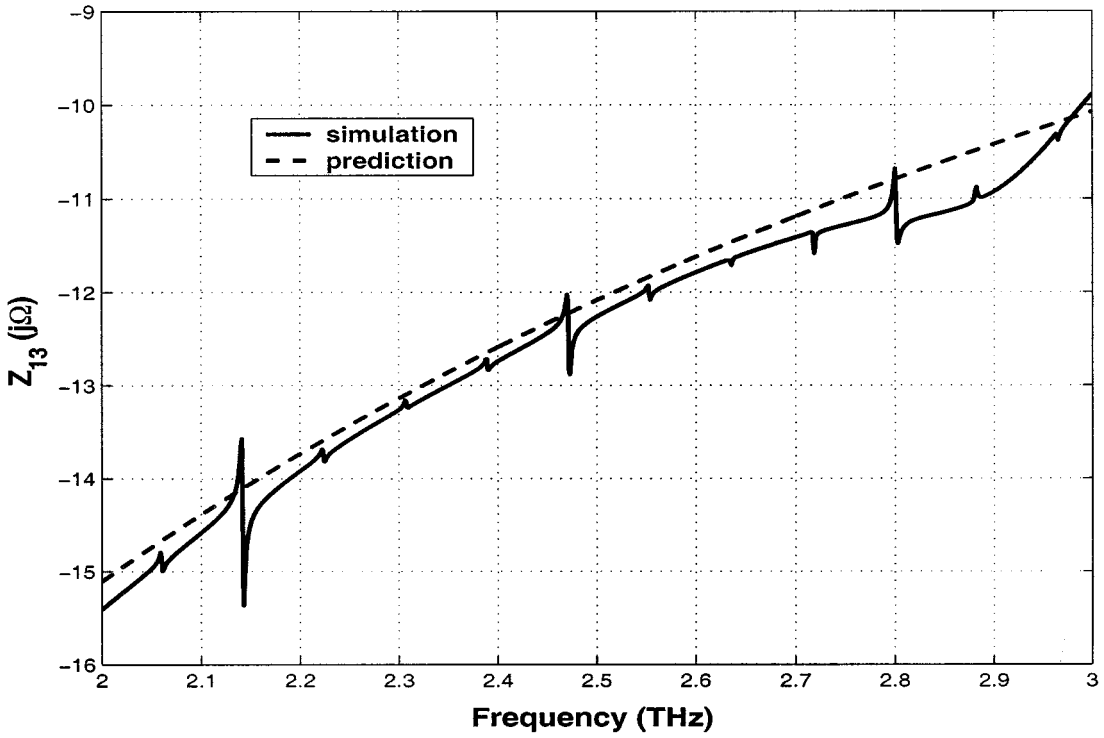

Fig. 9. Simulation (solid line) and predicted (dashed line) results of Z_{13} for the EA255 sample.

For antenna matching purposes, the behavior of Z_{13} as a capacitor is not good. Assuming a bowtie antenna of self similar design connected between the top and bottom control gates as shown in Fig. 1, then its input impedance is about 74 Ω on top of a GaAs substrate. To have maximum coupling between the DELTT and the antenna, the DELTT impedance should be the complex conjugate of the antenna impedance. This suggests that connecting the antenna between the top and bottom control gates is not good and should be avoided. We propose connecting the antenna between the source and drain terminals. It should be mentioned here that connecting the antenna between the source and drain is as effective as connecting it between the top and bottom control gates, and the device should retain its full functionality. In this case the antenna will collect the THz radiation and transform into a voltage difference between the source and drain such that, with the correct photon energy (or THz frequency), resonant tunneling can be initiated between the two QWs. The location of the peak in the $*I$–V characteristic of the DELTT will be proportional to the source–drain voltage, which is in turn proportional to the frequency of the THz radia-

tion through the relation: $v_{SD} = V_{SD} + hf/e$, where V_{SD} is the dc voltage, h is Planck's constant, f is the frequency, and e is the electron charge. From Fig. 4, we see that a bowtie antenna of 74 Ω input impedance could be matched to the real part of Z_{SD} at some frequencies. However, the presence of a big inductive reactance in Z_{SD} complicates any further matching between the antenna and the DELTT. More investigation is required to see if it is possible to change the DELTT parameters and dimensions, or find a new antenna so that a better matching between the DELTT and the antenna can be obtained.

V. Conclusion

This paper presented a general equivalent circuit model for the DELTT device. Measurements at very high frequencies are not available since it is extremely difficult to obtain accurate measurements of impedance at such high frequencies. However, the presented circuit model, based on the most important physical interactions that affect the device operation, can be utilized at THz frequencies, assuming that the device parameters (like density and mobility) at these high frequencies can be determined accurately. Moreover, the simulations results of sample devices revealed that it is extremely difficult to match the DELTT impedance to the broadband band bowtie antenna impedance.

References

[1] J. M. Gering *et al.*, "A small-signal equivalent-circuit model for GaAs–$Al_xGa_{1-x}As$ resonant tunneling heterostructure at microwave frequencies," *J. Appl. Phys.*, vol. 61, pp. 271–276, Jan. 1987.

[2] H. Drexler, J. S. Scott, and S. J. Allen, "Photon-assisted tunneling in a resonant tunneling diode: Stimulated emission and absorption in the THz range," *Appl. Phys. Lett.*, vol. 67, no. 19, pp. 2816–2818, Nov. 1995.

[3] J. A. Simmons *et al.*, "Planar quantum transistor based on 2D–2D tunneling in double quantum well heterostructure," *J. Appl. Phys.*, vol. 84, no. 10, pp. 5626–5634, Nov. 1998.

[4] M. A. Blout *et al.*, "Double Electron Layer Tunneling Transistor (DELTT)," *Semicond. Sci. Technol.*, vol. 13, pp. A180–A183, 1998.

[5] J. S. Moon *et al.*, "Unipolar complementary circuits using double electron layer tunneling transistor," *Appl. Phys. Lett.*, vol. 74, pp. 314–316, Jan. 1999.

[6] Y. Katayama and D. C. Tsui, "Lumped circuit model of two-dimensional to two-dimensional tunneling transistors," *Appl. Phys. Lett.*, vol. 62, no. 20, pp. 2563–2565, May 1993.

[7] P. J. Burke, I. B. Spielman, and J. P. Eisenstein, "High frequency conductivity of the high-mobility two-dimensional electron gas," *Appl. Phys. Lett.*, vol. 76, pp. 745–747, Feb. 2000.

[8] P. J. Burke and J. P. Eisenstein, "Interlayer plasmons,", to be published.

[9] A. G. Derneryd, "Analysis of microstrip disk antenna element," *IEEE Trans. Antennas Propagat.*, vol. 27, pp. 660–664, Sept. 1979.

[10] D. M. Pozar, *Microwave Engineering*, 2nd ed: Wiley, 1998.

[11] R. S. Elliot, *An Introduction to Guided Waves and Microwave Circuits*. Englewood Cliffs, NJ: Prentice-Hall, 1993.

[12] R. E. Collin, *Foundations for Microwave Engineering*. New York: McGraw-Hill, 1992.

Majid M. Khodier (M'01) received the B.Sc. and M.Sc. degrees from Jordan University of Science and Technology, Irbid, Jordan, and the Ph.D. degree from the University of New Mexico, Albuquerque, all in electrical engineering, in 1995, 1997, and 2001, respectively.

He worked as a Postdoctoral Researcher in the Department of Electrical Engineering, Univerisity of New Mexico, where he performed research in the areas of RF/photonic antennas for wireless communications, modeling of MEMS switches for multiband antennas for wireless communications, and modeling of MEMS switches for multiband antenna applications. In September of 2002, he joined the Department of Electrical Engineering, Jordan University of Science and Technology, as an Assistant Professor. His research interests include the areas of numerical techniques in electromagnetics (FDTD, MoM), modeling of passive and active microwave components and circuits, applications of MEMS in antennas, and RF/Photonic antenna applications in broadband wireless communications.

Dr. Khodier serves as a reviewer for IEEE Transactions on Antennas and Propagation.

Christos G. Christodoulou (M'80–SM'90–F'02) received the B.Sc. degree in physics and math from the American University of Cairo, Cairo, Egypt, in 1979, and the M.S. and Ph.D. degrees in electrical engineering from North Carolina State University, Raleigh, in 1981 and 1985, respectively.

He served as a faculty member in the University of Central Florida, Orlando, from 1985 to 1998, where he received numerous teaching and research awards. In 1999, he joined the faculty of the Electrical and Computer Engineering Department of the University of New Mexico, Albuquerque, as a Chair. He has published over 160 papers in journals and conferences. He is an Associate Editor for *IEEE AP Magazine*, and the *ACES Journal*. His research interests are in the areas of antennas, high power microwaves, modeling of electromagnetic systems, and neural network applications in electromagnetics.

Dr. Christodoulou serves as an Associate Editor for the IEEE Transactions on Antennas and Propagation.

Jerry A. Simmons received the B.A. degree in philosophy and physics from New College of Florida, Sarasota, in 1982, and the M.A. and Ph.D. degrees from Princeton University, Princeton, NJ, both in electrical engineering in 1986 and 1990, respectively.

From 1982 to 1984, he was a Technician at Bell Laboratories, Murray Hill, NJ. He joined Sandia National Laboratories in 1990, in the Department of Semiconductor Physics. From 1990 to 2000, he progressed through the positions of Member, Senior Member, and Principal Member of Technical Staff, working in the areas of the integer and fractional quantum Hall effect, quantum transport in double quantum well heterostructures, single-electron transistors, and novel THz detectors based on photon-assisted tunneling. In 2000, he was appointed Manager of the Semiconductor Material and Device Sciences Department, where he now oversees numerous efforts in nanoelectronics and nanophotonics, and leads Sandia's solid-state lighting program. He has authored over 80 publications.

Dr. Simmons won an Industry Week Technology of the Year Award for a tunneling transistor in 1998. He is a member of the American Physical Society.